JOURNAL OF MATHEMATICAL PHYSICS **55**, 061501 (2014)

Asymptotic solution of light transport problems in optically thick luminescent media

Derya Şahin-Biryol[a] and Boaz Ilan
Applied Mathematics Unit, School of Natural Sciences, University of California Merced, 5200 North Lake Road, Merced, California 95343, USA

(Received 4 December 2013; accepted 29 May 2014; published online 20 June 2014)

We study light transport in optically thick luminescent random media. Using radiative transport theory for luminescent media and applying asymptotic and computational methods, a corrected diffusion approximation is derived with the associated boundary conditions and boundary layer solution. The accuracy of this approach is verified for a plane-parallel slab problem. In particular, the reduced system models accurately the effect of reabsorption. The impacts of varying the Stokes shift and using experimentally measured luminescence data are explored in detail. The results of this study have application to the design of luminescent solar concentrators, fluorescence medical imaging, and optical cooling using anti-Stokes fluorescence. © *2014 AIP Publishing LLC*. [http://dx.doi.org/10.1063/1.4882815]

I. INTRODUCTION

Most studies of light propagation in random media assume that the light scatters **elastically**, i.e., the wavelength, which is inversely proportional to energy, does not change as a result of its interaction with the medium. Such systems are commonly modeled using (single-energy) radiative transport theory, also called radiative transfer.[1–3] In contrast, when light propagates in a luminescent medium, it scatters **inelastically**, i.e., the emitted wavelength differs from the absorbed one. Inelastic scattering in random media can be modeled using multi-energy radiative transfer, which has been applied, among other problems, to model the scattering of neutrons, neutrinos, and other massive particles, as well as non-resonant scattering of photons (cf. Refs. 4–7). An important aspect of luminescence, e.g., fluorescence or phosphorescence, is that the absorbed and reemitted spectra are anchored to atomic or molecular resonances. As a result, there can be a significant overlap between the absorption and reemission spectra. This overlap induces **reabsorption**, i.e., light that is absorbed and reemitted, can be reabsorbed. Since the probability of reemission is strictly less than one, multiple reabsorption can result in a significant loss of light flux. Reabsorption is a limiting factor for fluorescence medical imaging (cf. Refs. 8–11), optical cooling using anti-Stokes fluorescence (cf. Refs. 12 and 13), and luminescent solar concentrators (**LSCs**) (cf. Refs. 14 and 15). For this reason, it is important to model accurately the effects of reabsorption.

A common method for computing transport in multi-energy systems is Monte Carlo simulations. This approach has been applied to luminescent media as well (cf. Refs. 11, 14, 16, and 17). However, Monte Carlo simulations converge relatively slowly. On the other hand, almost all previous studies of luminescence in random media that have used the deterministic radiative transfer approach have modeled the physical system using two coupled single-wavelength radiative transport equation **(RTEs)**, which correspond, in some average sense, to the absorption (excitation) and reemission (fluorescence) (cf. Refs. 18–27). Furthermore, almost all of these studies have considered optically thick media and derived a diffusion approximation (DA) consisting of two coupled partial differential equations. While this approach is certainly useful, a limitation of this approach is that it does not model reabsorption accurately.

[a]Electronic mail: dsahin@ucmerced.edu

Recently, the authors proposed a deterministic "luminescence radiative transport equation" (**LRTE**) for modeling light scattering in random luminescent media (**LSCs**)[28] (see also Ref. 29 for a similar equation). The LRTE is an instance of a multi-energy (or multi-wavelength) radiative transfer theory. This theory accounts accurately for reabsorption and has been used to model light transport in LSCs.[28] However, solving the LRTE can be computationally challenging. The aim of this study is to develop an asymptotic theory for the LRTE in optically thick media. This regime is characterized by reemission probability (photoluminescence quantum yield) close to unity. Using asymptotic methods, we derive a corrected diffusion approximation, which consists of a single partial differential equation, with associated boundary conditions and a boundary layer solution. The accuracy of this approach is verified for a plane-parallel slab problem by comparison with direct computations of the LRTE. In particular, within the regime of asymptotic validity, the reduced system accounts accurately for reabsorption.

The paper is organized as follows. In Sec. II, we recap the LRTE and associated boundary conditions. In Sec. III, starting with the LRTE in its scaled form [Eqs. (9) and (12)] and using asymptotic methods, a diffusion approximation is derived including the interior and boundary layer solutions. In Sec. IV, the plane-parallel slab problem is solved for the special case when the incident light is a collimated beam. In particular, we show that the reduced system captures accurately the reabsorption of light. In Sec. V, the validity of the diffusion approximation is verified by comparison with direct computation of the LRTE. The impact of varying the Stokes shift, i.e., the mean wavelength separation between the absorption and reemission spectra, is investigated in Sec. V A. To systematically analyze various physical assumptions and regimes, we employ "synthetic" luminescence data in the form of Gaussian distributions. In addition, in Sec. V B we test the reliability of the diffusion approximation using experimentally measured luminescence data.

II. LUMINESCENCE RADIATIVE TRANSPORT EQUATION

The fundamental quantity in radiative transfer is radiance (or specific intensity), which is the power per projected surface area, per unit wavelength, per unit direction. We consider steady state systems (i.e., no time dependence) and denote the radiance by

$$I(\mathbf{x}, \Omega, \lambda) : \mathfrak{D} \times \mathbf{S}^2 \times \Lambda \to \mathbb{R}^+,$$

where $\mathfrak{D} \subset \mathbb{R}^3$ is the spatial domain, $\mathbf{S}^2$ the unit sphere of directions, Λ the interval of wavelengths participating in the process, and $\mathbb{R}^+ \equiv \mathbb{R} \bigcap \{f | f \geq 0\}$. Following Ref. 28, we assume that the radiance is governed by the LRTE

$$\Omega \cdot \nabla I + \mu_a \mathcal{L}_a I = \mu_r \mathcal{L}_r I, \tag{1}$$

where $\mathcal{L}_a$ and $\mathcal{L}_r$ are the absorption and reemission operators (defined below), respectively, and μ_a and μ_r are the absorption and the reemission constants, respectively. These constants are related by

$$\mu_r = \mathrm{QY} \mu_a, \tag{2}$$

where QY is the photoluminescence quantum yield, which is the probability that a photon that is absorbed will be reemitted. The absorption spectrum is denoted by $f_a(\lambda)$, which is the probability of absorption at a particular wavelength, i.e., $\lambda \mapsto f_a(\lambda) \in \mathbb{R}^+$ is a probability distribution function with the usual normalization $\int_\Lambda f_a(\lambda) d\lambda = 1$. The absorption operator in (1) is defined as

$$\mathcal{L}_a I = f_a(\lambda) I. \tag{3}$$

The general reemission operator in (1) is

$$\mathcal{L}_r I = \int_\Lambda \int_{\mathbf{S}^2} K_r(\lambda, \lambda', \Omega, \Omega') I(\mathbf{x}, \Omega', \lambda') \, d\Omega' d\lambda', \tag{4}$$

where $K_r(\lambda, \lambda', \Omega, \Omega'; g)$ is the reemission kernel. The reemission kernel is the probability of light that is absorbed in direction Ω' and wavelength λ' to be reemitted in direction Ω and wavelength λ. The reemission kernel proposed in Ref. 28 for luminescence is

$$K_r(\lambda, \lambda', \Omega, \Omega'; g) = f_r(\lambda) f_a(\lambda') P_r(\Omega, \Omega'), \tag{5}$$

where $P_r(\Omega, \Omega')$ is called the scattering phase function (defined below) and $f_r(\lambda)$ is the normalized reemission spectrum $[\int_\Lambda f_r(\lambda)\, d\lambda = 1]$. To model the scattering phase function, we use the Henyey-Greenstein function[30]

$$P_r(\Theta; g) = \frac{1}{4\pi} \frac{1 - g^2}{\left(1 - 2g\cos\Theta + g^2\right)^{3/2}}, \quad \cos\Theta \doteq \Omega \cdot \Omega' \in [-1, 1], \tag{6}$$

where $g \in [0, 1]$ is the anisotropy parameter. This function determines the amount of light scattered at a relative angle Θ with respect to the direction of incidence. We note that the reemission kernel (5) agrees with Monte Carlo modeling of photon transport in luminescent media.[28]

For a well-posed problem, the boundary conditions for (1) are

$$I = \mathcal{R}I + \mathfrak{B} \quad \text{on} \quad \Gamma_{in} = \{(\mathbf{x}, \Omega, \lambda) \in \partial\mathfrak{D} \times \mathbf{S}^2 \times \Lambda,\ \Omega \cdot \hat{n} < 0\}. \tag{7}$$

These conditions prescribe the radiance at the spatial boundary for all directions pointing into the domain, i.e., along the unit outward normal $\hat{n}$. Here, $\mathfrak{B}$ denotes the exterior source incident on the boundary, such as sunlight or a probe beam, and $\mathcal{R}$ is the Fresnel reflection operator for the light reflected internally at the boundary due to a mismatch in the refractive indices inside and outside of the domain.

It is interesting to point out that the (single-wavelength) RTE is a special case of (1) with the special reemission kernel

$$K_r(\lambda, \lambda', \Omega, \Omega') = \delta(\lambda - \lambda')P_r(\Omega, \Omega'), \tag{8}$$

where δ is the Dirac delta function. However, unlike (8), the luminescence reemission kernel (5) is a function of the **product** of absorption and reemission spectra. Physically, this is because the absorbed and reemitted spectra of luminescence are anchored to atomic or molecular resonances. In contrast, **non-resonant** inelastic scattering of massive particles and/or photons is characterized by a scattering cross section that depends on the relative energy or wavelength difference between the incident and scattered radiation. In some cases (such as Compton scattering), the energy loss is a function of the scattering angle as well. The corresponding scattering kernels are therefore modeled by functions of $(E - \alpha E' - \beta\Omega \cdot \Omega')$, where E and E' are the incident and scattered energies (or frequencies), respectively, and α and β are constants (cf. Refs. 4, 7, and 31). Moreover, the energy loss in non-resonant scattering is often small. In such cases, the multi-energy RTE can be approximated with a reduced Fokker-Planck type equation (cf. Refs. 4 and 7). However, such an approximation is in general not valid for luminescence.

III. DIFFUSION APPROXIMATION IN OPTICALLY THICK MEDIA

Radiative transport equations are difficult to solve without introducing approximations. In optically thick media, or in highly scattering media, the (time-independent) radiative transfer equation can be approximated with an elliptic partial differential equation, which is called the **DA** (cf. Refs. 3, 32–35). The diffusion approximation is much simpler than the RTE, because it is local and does not depend on direction. However, it is well-known that the standard diffusion approximation is not very accurate near the boundaries of the domain (cf. Refs. 36–40). Many studies have addressed this limitation using various other methods. Larsen and Keller[41–43] used boundary layer matched asymptotic expansion techniques to derive an equation for the boundary layer. Kim[44] improved upon this earlier work by introducing a corrected diffusion approximation and boundary layer. In this study, following the Kim's approach, we derive asymptotically a corrected diffusion approximation for the LRTE (1). Here, we refer to the approximation in the interior of the domain as the (corrected) diffusion approximation, whereas, the full approximation including the boundary layer solution is referred to as the "diffusion approximation with a boundary layer" or **DABL** (see Fig. 1).

Before introducing the asymptotic analysis, it is convenient to regroup the terms in the LRTE (1) as

$$\Omega \cdot \nabla I + \underbrace{\mu_a(1 - \mathrm{QY})\, f_a(\lambda) I}_{\text{absorption}} + \underbrace{\mu_a \mathrm{QY}\, f_a(\lambda)\mathcal{L}I}_{\text{reemission}} = 0, \tag{9}$$

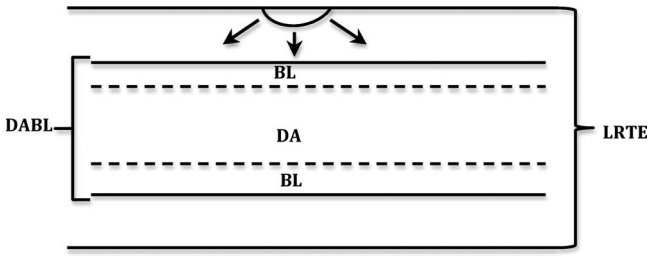

FIG. 1. A schematic representation of regions of validity for of the diffusion approximation (DA) and boundary layer (BL).

where

$$\mathcal{L}I \doteq I - \frac{f_r(\lambda)}{f_a(\lambda)} \int_{\mathbf{S}^2} \int_{\Lambda} P_r(\Omega \cdot \Omega') f_a(\lambda') I d\lambda' d\Omega'. \tag{10}$$

Assumption 1. We make the following physical assumptions about the medium and source terms.

1. *The medium has a quantum yield close to unity, i.e.,*
$$\mathrm{QY} = 1 - \epsilon^2, \quad 0 < \epsilon \ll 1. \tag{11}$$
2. *The absorption constant is* $\mu_a = \dfrac{\alpha}{\epsilon}$, *where* $\alpha = \mathcal{O}(1)$ *is a rescaled absorption constant.*
3. *The absorption and reemission spectra scale as* $f_a = \mathcal{O}(1)$ *and* $f_r = \mathcal{O}(1)$.
4. *The spatial variations of the incident source and of the boundary of the domain are small compared with* ϵ.

Assumption (1) is suitable for many organic and semiconductor fluorescent particles, whose quantum yield can be as high as 95% or higher (cf. Refs. 14 and 15). The other assumptions ensure that the validity of the asymptotic scaling (cf. Refs. 41 and 43 for a detailed discussion of the smoothness assumptions).

Introducing these assumptions into (9) leads to

$$\epsilon \Omega \cdot \nabla I + \epsilon^2 \alpha f_a(\lambda) I + (1 - \epsilon^2) \alpha f_a(\lambda) \mathcal{L} I = 0. \tag{12}$$

This equation is our starting point of the asymptotic analysis.

A. Asymptotic analysis

We seek an approximate solution of (12) with the boundary condition (7) in the form

$$I_{\mathrm{DABL}} \approx \Phi_{int} + \Psi_{BL}, \tag{13}$$

where Φ_{int} is the interior solution, i.e., the corrected diffusion approximation, and Ψ_{BL} is the boundary layer solution.

1. Corrected diffusion approximation for the interior solution

In the interior of the domain, we expand the solution as

$$\Phi_{int} = \phi_0 + \epsilon \phi_1 + \cdots. \tag{14}$$

Substituting (14) into (12) and collecting in powers of ϵ, leads to

$$-\alpha f_a(\lambda) \mathcal{L} \phi_k = \Omega \cdot \nabla \phi_{k-1} + \alpha f_a(\lambda) [\mathbb{I} - \mathcal{L}] \phi_{k-2}, \quad k = 0, 1, \ldots, \tag{15}$$

where $\mathbb{I}$ is the identity operator and it is implied that $\phi_{-2} = \phi_{-1} \equiv 0$. For $k = 0$, the leading order equation in (15) is

$$\mathcal{L} \phi_0 = 0. \tag{16}$$

Using (10) and (16) gives

$$\phi_0 = \frac{f_r(\lambda)}{f_a(\lambda)} \int_{\mathbf{S}^2} \int_{\Lambda} P_r(\Omega \cdot \Omega') f_a(\lambda') \phi_0 d\Omega' d\lambda'. \tag{17}$$

Since the right-hand side does not depend on Ω, ϕ_0 does not depend on Ω,

$$\phi_0 = \phi_0(\mathbf{x}, \lambda). \tag{18}$$

In other words, the eigenfunction of $\mathcal{L}$ corresponding to the zero eigenvalue is an isotropic function, For $k = 1$, Eq. (15) gives

$$-\alpha f_a(\lambda) \mathcal{L}\phi_1 = \Omega \cdot \nabla \phi_0. \tag{19}$$

We seek a solution of the form

$$\phi_1 = \frac{C}{f_a(\lambda)} \Omega \cdot \nabla \phi_0, \tag{20}$$

where C is the undetermined constant. Substituting (20) into (19) leads to

$$-\alpha C \Omega \cdot \nabla \phi_0 + \alpha C f_r(\lambda) \int_{\Lambda} \int_{\mathbf{S}^2} P_r(\Omega \cdot \Omega') \Omega' \cdot \nabla \phi_0 d\Omega' d\lambda' = \Omega \cdot \nabla \phi_0. \tag{21}$$

To continue we need a certain identity. It can be shown that for any function, $P_r(\Omega \cdot \Omega')$, and any vector function $\mathbf{F}(\cdot)$ that does not depend on Ω, the following identity holds (cf. Ref. 3):

$$\int P_r(\Omega \cdot \Omega') \Omega' \cdot \mathbf{F} d\Omega' = g \Omega \cdot \mathbf{F}, \tag{22}$$

where the integration is over all directions and g, the anisotropy parameters, is the first moment of P_r, i.e.,

$$g = \int_{-1}^{1} P_r(\Theta) \cos \Theta d\Theta,$$

where we have used the notation in (6).

Using (22) with $\mathbf{F} = \nabla \phi_0$, Eq. (21) simplifies to

$$\alpha C \Omega \cdot \nabla \phi_0 - \alpha f_r(\lambda) C g \Omega \cdot \int_{\Lambda} \nabla \phi_0 d\lambda' = -\Omega \cdot \nabla \phi_0. \tag{23}$$

Integrating (23) over Λ, using $\int_{\Lambda} f_r(\lambda) d\lambda = 1$, and rearranging the terms leads to

$$\int_{\Lambda} d\lambda \left[1 + C\alpha(1-g)\right] \Omega \cdot \int_{\Lambda} \nabla \phi_0 d\lambda' = 0. \tag{24}$$

Since ϕ_0 is isotropic and its gradient is nonzero, Eq. (24) yields the undetermined constant as

$$C = -\frac{1}{\alpha(1-g)}. \tag{25}$$

Using (20), the first-order correction term is

$$\phi_1 = -\frac{1}{\alpha(1-g) f_a(\lambda)} \Omega \cdot \nabla \phi_0. \tag{26}$$

For $k = 2$, Eq. (15) gives

$$\Omega \cdot \nabla \phi_1 + \alpha f_a(\lambda) [\mathbb{I} - \mathcal{L}] \phi_0 = -\alpha f_a(\lambda) \mathcal{L} \phi_2. \tag{27}$$

Substituting $\mathcal{L}\phi_0 = 0$ and (26) we get

$$\Omega \cdot \nabla \cdot \left[-\frac{\Omega \cdot \nabla \phi_0}{\alpha(1-g) f_a(\lambda)} \right] + \alpha f_a(\lambda) \phi_0 = -\alpha f_a(\lambda) \mathcal{L} \phi_2. \tag{28}$$

Next, we integrate both sides over $\mathbf{S^2} \times \Lambda$. Regarding the right-hand side, we recall that

$$\mathcal{L}\phi_2 = \phi_2 - \frac{f_r(\lambda)}{f_a(\lambda)} \int_{\mathbf{S^2}} \int_{\Lambda} P_r(\Omega \cdot \Omega') f_a(\lambda') \phi_2 d\Omega' d\lambda'. \tag{29}$$

Multiplying $\mathcal{L}\phi_2$ by $f_a(\lambda)$ and integrating over $\mathbf{S^2} \times \Lambda$ gives

$$\int_{\Lambda} \int_{\mathbf{S^2}} f_a(\lambda) \mathcal{L}\phi_2 \, d\Omega d\lambda = \int_{\Lambda} \int_{\mathbf{S^2}} f_a(\lambda) \phi_2 \, d\Omega d\lambda - \int_{\Lambda} f_r(\lambda) d\lambda \int_{\mathbf{S^2}} P_r(\Omega \cdot \Omega') \, d\Omega \int_{\Lambda} \int_{\mathbf{S^2}} f_a(\lambda) \phi_2 \, d\Omega d\lambda.$$

Since $\int_{\Lambda} f_r(\lambda) d\lambda = 1$ and $\int_{\mathbf{S^2}} P_r(\Omega \cdot \Omega') \, d\Omega = 1$, it follows that the right-hand side is zero. Hence, the double integral of the right-hand side of (28) vanishes. Using the divergence theorem for the left-hand side of (28) leads to

$$\int_{\Lambda} [\nabla \cdot (\kappa \nabla \phi_0) - \alpha f_a(\lambda) \phi_0] \, d\lambda = 0, \tag{30}$$

where the diffusion coefficient is

$$\kappa(\lambda) = \frac{1}{3(1-g)\alpha f_a(\lambda)}. \tag{31}$$

In order to obtain a unique solution of (30) subject to the boundary conditions (7), a sufficient condition is to require that the integrand of (30) vanishes, i.e.,

$$\nabla \cdot (\kappa \nabla \phi_0) - \alpha f_a(\lambda) \phi_0 = 0. \tag{32}$$

Thus, to $\mathcal{O}(\epsilon)$, the interior solution Φ_{int} is

$$\Phi_{int} \sim \phi_0 - 3\kappa\epsilon \Omega \cdot \nabla \phi_0, \tag{33}$$

where ϕ_0 satisfies (32). This is the corrected diffusion approximation.

We remark that the "standard" diffusion approximation is

$$\Phi_{DA} \sim \phi_0, \tag{34}$$

i.e., the solution of (32) alone. It is important to note that, for the solution of (32) to be correct to $\mathcal{O}(\epsilon)$ near the boundary of the domain and in its interior, the boundary conditions for (32) must be asymptotically accurate to $\mathcal{O}(\epsilon)$ as well. In Sec. IV C, we derive such boundary conditions for the plane-parallel problem.

2. Boundary layer solution

In the boundary layer, we seek an approximate solution Ψ_{BL} of (12) in a neighborhood of a particular point $\mathbf{x}_b$ on the smooth boundary of $\partial\mathfrak{D}$. To do this, a new coordinate system is defined with $\mathbf{x}_b$ at the origin and $\mathbf{x} \mapsto (\boldsymbol{\rho}, \zeta)$, where $\zeta \parallel \hat{n}(\mathbf{x}_b)$ and $\boldsymbol{\rho} \perp \hat{n}(\mathbf{x}_b)$. Accordingly, the new angular variables are defined as

$$\mu = \Omega \cdot \hat{n}(\mathbf{x}_b) = \cos\theta, \quad \mu \in [-1, 1], \tag{35}$$

$$\Omega_{\perp} = \sqrt{1-\mu^2}(\cos\varphi, \sin\varphi), \quad \varphi \in [-\pi, \pi]. \tag{36}$$

Thus, $\Psi_{BL} = \Psi_{BL}(\boldsymbol{\rho}, \zeta, \mu, \Omega_{\perp}, \lambda)$.

We consider the source term on $\partial\mathfrak{D}$, i.e., at $\zeta = 0$, to be a slowly varying and axisymmetric about $\hat{n}(\mathbf{x}_b)$ for all $\mathbf{x}_b \in \partial\mathfrak{D}$. Therefore, using the notation of (7), the boundary source term is denoted as $\mathfrak{B}(\boldsymbol{\rho}, \mu, \lambda)$, i.e., independent of $\Omega_{\perp}$. Similarly, the Fresnel reflection operator in (7) is assumed to be axisymmetric and

$$\mathcal{R}[I(\mu, \cdot)] \equiv r(\mu) I(-\mu, \cdot), \tag{37}$$

where $r(\mu)$ is the reflection coefficient. As $I \approx \Phi_{int} + \Psi_{BL}$, the boundary condition on $\zeta = 0$ can be written as

$$\Psi_{BL}(\boldsymbol{\rho}, 0, \mu, \Omega_\perp, \lambda) = -\Phi_{int}(\boldsymbol{\rho}, 0, \mu, \lambda) + r(\mu)\Psi_{BL}(\boldsymbol{\rho}, 0, -\mu, \Omega_\perp, \lambda) + r(\mu)\Phi_{int}(\boldsymbol{\rho}, 0, -\mu, \lambda) + \mathfrak{B}(\boldsymbol{\rho}, \mu, \lambda).$$

Substituting the interior solution (33) yields

$$\Psi_{BL}(\boldsymbol{\rho}, 0, \mu, \lambda) = -\phi_0(\boldsymbol{\rho}, 0, \lambda) + 3\kappa\epsilon(\mu\partial_\zeta + \Omega_\perp \cdot \nabla_\perp)\phi_0(\boldsymbol{\rho}, 0, \lambda) + r(\mu)\Psi_{BL}(\boldsymbol{\rho}, 0, -\mu, \lambda)$$
$$+r(\mu)\phi_0(\boldsymbol{\rho}, 0, \lambda) - 3\kappa\epsilon r(\mu)\left[-\mu\partial_\zeta + \Omega_\perp \cdot \nabla_\perp\right]\phi_0(\boldsymbol{\rho}, 0, \lambda) + \mathfrak{B}(\boldsymbol{\rho}, \mu, \lambda) \quad \text{at} \quad \zeta = 0, \tag{38}$$

where we have used the operator identity

$$\Omega \cdot \nabla \equiv \mu\partial_\zeta + \Omega_\perp \cdot \nabla_\perp, \tag{39}$$

where $\nabla_\perp$ denotes the gradient on the tangent space of $\partial\mathfrak{D}$.

We now introduce the stretched variable $\zeta = \epsilon\zeta^*$. Substituting (36) into (12) and using (39) with the stretched variable gives

$$\mu\frac{\partial\Psi_{BL}}{\partial\zeta^*} + \epsilon\Omega_\perp\nabla_\perp\Psi_{BL} + \epsilon^2\alpha f_a\Psi_{BL} + (1-\epsilon^2)\alpha f_a\mathcal{L}\Psi_{BL} = 0. \tag{40}$$

We seek a solution of (40) as $\epsilon \to 0^+$. For fixed ζ, this means that $\zeta^* \to \infty$. Therefore, the boundary layer problem is defined in the half space $\zeta^* > 0$. A necessary condition to ensure the asymptotic matching between the interior and boundary layer solutions is

$$\Psi_{BL} \to 0 \quad \text{as} \quad \zeta^* \to \infty. \tag{41}$$

Similar to the interior solution, we seek a solution in the boundary layer of the form

$$\Psi_{BL}(\boldsymbol{\rho}, \epsilon\zeta^*, \mu, \Omega_\perp, \lambda) = \psi_0 + \epsilon\psi_1 + \mathcal{O}(\epsilon^2). \tag{42}$$

Substituting (42) into (40) and collecting the $\mathcal{O}(1)$ and $\mathcal{O}(\epsilon)$ terms, gives the following two equations in the half-space $\zeta^* > 0$:

$$\mu\frac{\partial\psi_0}{\partial\zeta^*} + \alpha f_a\mathcal{L}\psi_0 = 0, \tag{43}$$

$$\mu\frac{\partial\psi_1}{\partial\zeta^*} + \alpha f_a\mathcal{L}\psi_1 = \Omega_\perp \cdot \nabla_\perp\psi_0. \tag{44}$$

Substituting (42) into the boundary conditions (38) and collecting the $\mathcal{O}(1)$ and $\mathcal{O}(\epsilon)$ terms, yields the associated boundary conditions on $\zeta^* = 0$ as

$$\psi_0(\boldsymbol{\rho}, 0, \mu, \Omega_\perp, \lambda) = r(\mu)\psi_0(\boldsymbol{\rho}, 0, -\mu, \Omega_\perp, \lambda) - [1 - r(\mu)]\phi_0(\boldsymbol{\rho}, 0, \lambda) + \mathfrak{B}(\boldsymbol{\rho}, \mu, \lambda), \tag{45}$$

$$\psi_1(\boldsymbol{\rho}, 0, \mu, \Omega_\perp, \lambda) = r(\mu)\psi_1(\boldsymbol{\rho}, 0, -\mu, \Omega_\perp, \lambda) + 3\kappa[1 + r(\mu)]\mu\frac{\partial\phi_0(\boldsymbol{\rho}, 0, \lambda)}{\partial\zeta^*} + 3\kappa[1 - r(\mu)]\Omega_\perp \cdot \nabla_\perp\phi_0(\boldsymbol{\rho}, 0, \lambda). \tag{46}$$

We observe that since (43) and (45) have only axisymmetric operators, the leading order solution ψ_0 does not depend on $\Omega_\perp$. In addition, by integrating (44) with respect to φ [defined in (36)] we observe that the term on the right-hand side vanishes. Similarly, integrating (46) with respect to φ we observe that the last term on the right-hand side vanishes. It follows that ψ_1 does not depend on φ (or $\Omega_\perp$).

Using (42), we conclude that, to $\mathcal{O}(\epsilon)$, $\Psi_{BL} = \Psi_{BL}(\boldsymbol{\rho}, \zeta, \mu, \lambda)$ does not depend on $\Omega_\perp$ and it satisfies the boundary value problem

$$\mu\frac{\partial\Psi_{BL}}{\partial\zeta^*} + \alpha f_a\mathcal{L}\Psi_{BL} = 0 \quad \text{in} \quad \zeta^* > 0, \tag{47a}$$

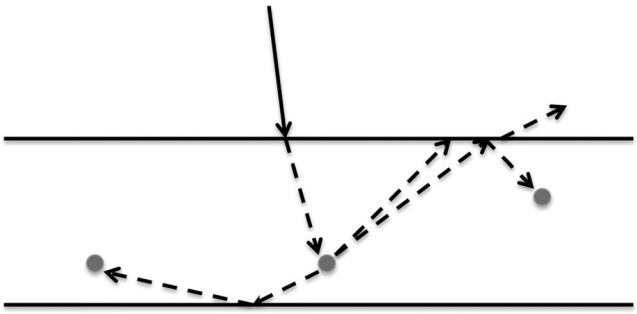

FIG. 2. A plane-parallel slab with a reflecting bottom surface at $z = z_1$ and transparent top surface at $z = 0$.

with the boundary conditions

$$\Psi_{BL}(\boldsymbol{\rho}, 0, \mu, \lambda) - r(\mu)\Psi_{BL}(\boldsymbol{\rho}, 0, -\mu\lambda) = \mathcal{S}(\boldsymbol{\rho}, \mu, \lambda), \quad \text{on } 0 < \mu \leq 1, \tag{47b}$$

where we have combined the non-homogeneous terms into

$$\mathcal{S}(\boldsymbol{\rho}, \mu, \lambda) \doteq -[1 - r(\mu)]\phi_0(\boldsymbol{\rho}, 0, \lambda) + \mathfrak{B}(\boldsymbol{\rho}, \mu, \lambda) + 3\epsilon\kappa[1 + r(\mu)]\mu\frac{d\phi_0}{d\zeta^*}(\boldsymbol{\rho}, 0, \lambda). \tag{47c}$$

We point out that these boundary conditions, and the boundary layer solution, depend on the interior solution, ϕ_0, which, in turn, requires the (yet unprescribed) boundary conditions.

Since the approximate boundary layer solution is axisymmetric, it is convenient to rewrite the reemission operator in (47a) as

$$\mathcal{L}\Psi_{BL} = \Psi_{BL} - \frac{1}{2}\frac{f_r(\lambda)}{f_a(\lambda)}\int_\Lambda \int_{-1}^{1} p_0(\mu, \mu')f_a(\lambda')\Psi_{BL}d\mu' d\lambda', \tag{48}$$

where $p_0(\mu, \mu')$ is the redistribution function for the Henyey-Greenstein scattering, i.e.,

$$p_0(\mu, \mu') = \frac{1}{2\pi}\int_{-\pi}^{\pi} P_r\left(\mu\mu' + \sqrt{1-\mu^2}\sqrt{1-\mu'^2}\cos(\varphi - \varphi')\right)d(\varphi - \varphi'). \tag{49}$$

Here, $p_0(\mu, \mu')$ determines the fraction of light from a cone of angle μ' that is reemitted into a cone of angle μ. Alternatively, this function can be expressed as

$$p_0(\mu, \mu') = \frac{2}{\pi}\frac{1 - g^2}{\sqrt{\gamma_1 + \gamma_2}(\gamma_1 - \gamma_2)}E(k), \tag{50}$$

where

$$\gamma_1 = 1 + g^2 - 2g\mu\mu', \ \gamma_2 = 2g\sqrt{1-\mu^2}\sqrt{1-\mu'^2}, \ k = \frac{2\gamma_2}{\gamma_1 + \gamma_2}, \tag{51}$$

and $E(k)$ is the complete elliptic integral of the second kind.

IV. SOLUTION IN A PLANE-PARALLEL SLAB

In this section, we apply the foregoing theory to find the asymptotic solution in the case of a plane-parallel slab (see Fig. 2).

A. Plane waves

To solve the boundary layer problem (47), we use the method of plane waves following Ref. 45. The first step is to compute the plane wave solutions (in the full-plane) and the associated spectrum. To do this, we make the ansatz

$$\Psi_{BL}(\zeta^*, \mu, \lambda) = V(\mu, \lambda)e^{\eta\zeta^*}, \tag{52}$$

where η and $V(\mu, \lambda)$ are eigenvalues and eigenfunctions, respectively. Substituting (52) into (47a) gives the generalized eigenvalue problem

$$\mu\eta V(\mu, \lambda) + \alpha f_a(\lambda)\mathcal{L}V(\mu, \lambda) = 0. \tag{53}$$

It is helpful to discretize this problem. This is used to compute the spectrum and the plane waves solutions and, later, in order obtain the asymptotic boundary conditions for the diffusion approximation. We discretize the $\mathcal{L}$ operator (48) using the Gauss-Legendre quadrature rule

$$\int_{-1}^{1} p_0(\mu, \mu'; g)V(\mu, \lambda)d\mu' \approx \sum_{j=-M}^{M} p_0(\mu_j, \mu'_j)V(\mu_j, \lambda)w'_j, \tag{54}$$

where μ'_j and w'_j are the quadrature abscissas and weights, respectively, and M is the number of roots of the Legendre polynomials. We also discretize the wavelength interval Λ into N equally spaced nodes and use the Simpson quadrature formula, i.e.,

$$\int_{\Lambda} V(\mu, \lambda')d\lambda' \approx \sum_{\ell=1}^{N} V(\mu, \lambda_\ell)q_\ell, \tag{55}$$

where the q_js are the corresponding weights. Substituting (54) and (55) into the operator (48) and into the eigenvalue problem (53) leads to the discrete generalized eigenvalue problem

$$\left(\mu_j\eta_j + \alpha f_a^\ell\right) V_{j,\ell} = \alpha \frac{f_r^\ell}{f_a^\ell} \sum_{\ell=1}^{N} f_a^\ell \sum_{j=-M}^{M} p_0(\mu_j, \mu'_j; g)V_{j,\ell}w'_j q_\ell, \tag{56}$$

where $V_{j,\ell} = V(\mu_j, \lambda_\ell)$, $f_a^\ell = f(\lambda_\ell)$, and $f_r^\ell = f_r(\lambda_\ell)$.

It can be observed that the pairs $[\eta, V(\mu, \lambda)]$ and $[-\eta, V(-\mu, \lambda)]$ satisfy the same Eq. (53). Therefore, the plane wave solutions have the symmetry property

$$\eta_j = \eta_{-j}, \quad V_{-j}(\mu, \lambda) = V_j(-\mu, \lambda), \quad j = 0, \ldots, M.$$

Hence, the eigenvalues can be ordered as

$$\cdots < \eta_{-j} < \ldots < \eta_{-1} < \eta_0 < \eta_1 < \ldots < \eta_j < \cdots, \tag{57}$$

where $\eta_0 = 0$ corresponds to a constant eigenfunction, V_0.[46]

The associated full-plane Green's function $G(\zeta^*, \mu, \lambda; \mu', \zeta')$ satisfies

$$\mu\frac{\partial G}{\partial \zeta^*} + \alpha f_a(\lambda)\mathcal{L}G = \delta(\mu - \mu')\delta(\zeta^* - \zeta'), \quad \mu \in [-1, 1], \zeta^*, \zeta' \in (-\infty, \infty). \tag{58}$$

The solution of (58) can be obtained using the above plane waves as

$$G(\zeta^*, \mu, \lambda; \zeta', \mu') = \begin{cases} \sum_{j\geq 0} V_j(\mu, \lambda)e^{\eta_j(\zeta^* - \zeta')}V_j(\mu', \lambda), & \zeta^* < \zeta' \\ \sum_{j\geq 0} W_j(\mu, \lambda)e^{-\eta_j(\zeta^* - \zeta')}W_j(\mu', \lambda), & \zeta^* > \zeta', \end{cases} \tag{59}$$

where $W_j \doteq V_{-j}$.

B. Green's function for the boundary layer problem

Next, we denote the Green's function for (47a) in the upper-half plane $\zeta^* > 0$ as $H^0(\zeta^*, \mu, \lambda; \zeta', \mu')$, which satisfies

$$\mu\frac{\partial H^0}{\partial \zeta^*} + \alpha f_a(\lambda)\mathcal{L}H^0 = \delta(\mu - \mu')\delta(\zeta^* - \zeta'), \quad \mu \in (0, 1], \zeta^* > 0, \tag{60a}$$

$$H^0(0, \mu, \lambda; \zeta', \mu') = r(\mu)H^0(0, -\mu, \lambda; \zeta', \mu'), \quad 0 < \mu \leq 1, \tag{60b}$$

where (60b) corresponds to the homogeneous (left-hand side) part of (47b) on the top surface. The solution of (60a) can be expressed in terms of the full-plane Green's function as

$$H^0(\zeta^*, \mu, \lambda; \zeta', \mu') = G(\zeta^*, \mu, \lambda; \zeta', \mu') - \tilde{G}(\zeta^*, \mu, \lambda; \zeta', \mu'), \tag{61}$$

where $\tilde{G}(\zeta^*, \mu, \lambda; \zeta', \mu')$ satisfies the auxiliary problem

$$\mu \frac{\partial \tilde{G}}{\partial \zeta^*} + \alpha f_a(\lambda) \mathcal{L}\tilde{G} = 0, \tag{62a}$$

$$\tilde{G}(0, \mu, \lambda; \zeta', \mu') = G(0, \mu, \lambda; \zeta', \mu'). \tag{62b}$$

The solution of (62) can be obtained as a series of plane waves. Combining it with Eqs. (59) and (61) yields

$$H^0(\zeta^*, \mu, \lambda; \zeta', \mu') = \begin{cases} \sum_{j\geq 0} V_j(\mu, \lambda) e^{\eta_j(\zeta^* - \zeta')} V_j(\mu', \lambda) - \sum_{j\geq 0} W_j(\mu) e^{\eta_j \zeta^*} \sum_{p>0} C_{j,p} V_p(\mu', \lambda) e^{-\eta_p \zeta'}, & \zeta^* < \zeta' \\ \sum_{j\geq 0} W_j(\mu, \lambda) e^{-\eta_j(\zeta^* - \zeta')} W_j(\mu', \lambda) - \sum_{j\geq 0} W_j(\mu, \lambda) e^{\eta_j \zeta^*} \sum_{p>0} C_{j,p} V_p(\mu', \lambda) e^{-\eta_p \zeta'}, & \zeta^* > \zeta', \end{cases} \tag{63}$$

where $C_{j,p}$ are constants. Substituting (63) into the boundary condition (60b) yields the linear system of equations for the constants $C_{j,p}$ as

$$\sum_{j\geq 0} \left[W_j(\mu, \lambda) - r(\mu) V_j(\mu, \lambda) \right] C_{j,p} = \left[V_p(\mu, \lambda) - r(\mu) W_p(\mu, \lambda) \right], \quad 0 < \mu \leq 1, \, p > 0. \tag{64}$$

The solution of the upper-half plane problem is then

$$\Psi^0_{BL}(\zeta^*, \mu, \lambda) = \int_0^1 H^0(\zeta^*, \mu, \lambda; 0, \mu') \mathcal{S}(\mu', \lambda) \mu' d\mu', \tag{65}$$

where $\mathcal{S}(\mu', \lambda)$ are the non-homogeneous terms in the boundary condition (Eq. (47b)). Combining (63) and (65) gives the boundary layer solution as

$$\Psi^0_{BL}(\zeta^*, \mu, \lambda) = \sum_{j\geq 0} W_j(\mu, \lambda) e^{-\eta_j \zeta^*} \int_0^1 \left[W_j(\mu', \lambda) + \sum_{p>0} C_{j,p} V_p(\mu', \lambda) \right] \mathcal{S}(\mu', \lambda) \mu' d\mu'. \tag{66}$$

We note that the same approach can yield the Green's function in the lower-half plane, which, due to the symmetries of the problem, can be written as

$$H^1(\zeta^*, \mu, \lambda; \zeta', \mu') = H^0(\zeta_1 - \zeta^*, -\mu, \lambda; \zeta_1 - \zeta', \mu'), \quad \mu \in [-1, 0), \zeta^* < \zeta_1, \tag{67}$$

where $\zeta_1 \equiv z_1/\epsilon$. Below we use (67) to solve the boundary layer problem at the bottom of the slab.

C. Asymptotic boundary conditions

Recall that the asymptotic matching conditions require that Ψ_{BL} decay to zero as $\zeta^* \to \infty$ [Eq. (41)]. The only non-decaying term in (66) is the one corresponding to the zero eigenvalue with a constant solution ($j = 0$). Hence, it follows from (66) that a necessary condition to satisfy (41) is

$$\mathcal{P}\left[\mathcal{S}(\mu, \lambda)\right] \equiv \int_0^1 \left[W_0(\mu', \lambda) + \sum_{p>0} C_{0,p} V_p(\mu', \lambda) \right] \mathcal{S}(\mu', \lambda) \mu' d\mu' = 0, \tag{68}$$

i.e., this is a solvability condition for boundary layer solutions that decay to zero. Combining the solvability condition (68) and (47c) gives

$$\mathcal{P}\left[\mathfrak{B}(\mu, \lambda) - (1 - r(\mu)) \phi_0(0, \lambda) + 3\epsilon\kappa\mu (1 + r(\mu)) \frac{\partial}{\partial \zeta^*} \phi_0(0, \lambda) \right] = 0. \tag{69}$$

Using (69), the boundary conditions for the corrected diffusion approximation (32) can be written as

$$a\phi_0 - b\hat{n} \cdot \nabla \phi_0 = \mathcal{B}_0, \tag{70a}$$

$$\mathcal{B}_0 = \mathcal{P}[\mathfrak{B}(\mu, \lambda)], \tag{70b}$$

$$a = \mathcal{P}[1 - r(\mu)], \tag{70c}$$

$$b = 3\epsilon\kappa\mathcal{P}[\mu(1 + r(\mu))]. \tag{70d}$$

We remark that many studies in the optics and physics literature have suggested various ways of choosing boundary conditions for the diffusion approximation (cf. Refs. 47–49 and references therein). The advantage of the boundary conditions (70) is that they are asymptotically accurate to $\mathcal{O}(\epsilon)$.

D. Interior solution

In the interior layer, using (32) and (70) gives the boundary value problem for the interior of the slab as

$$\kappa\frac{\partial^2\phi_0}{\partial z^2} - \alpha f_a(\lambda)\phi_0 = 0 \quad \text{in } 0 < z < z_1, \tag{71a}$$

$$a\phi_0 - b\frac{\partial\phi_0}{\partial z} = \mathcal{B}_0 \quad \text{on } z = 0, \tag{71b}$$

$$a\phi_0 + b\frac{\partial\phi_0}{\partial z} = 0 \quad \text{on } z = z_1. \tag{71c}$$

The solution of (71) is

$$\phi_0(z, \lambda) = c_1\cosh(mz) + c_2\sinh(mz), \tag{72}$$

where the coefficients are

$$c_1 = \frac{\mathcal{B}_0}{c_0}[a\sinh(mz_1) + mb\cosh(mz_1)], \tag{73a}$$

$$c_2 = -\frac{\mathcal{B}_0}{c_0}[a\cosh(mz_1) + mb\sinh(mz_1)], \tag{73b}$$

$$c_0 = (a^2 - m^2b^2)\sinh(mz_1) + 2mba\cosh(mz_1), \tag{73c}$$

$$m^2 = \frac{\alpha f_a(\lambda)}{\kappa}. \tag{73d}$$

Substituting (72) and (73) into (33), yields the asymptotically accurate interior layer solution as

$$\Phi_{int} \sim [c_1 - \mu\epsilon 3\kappa m c_2]\cosh(mz) + [c_2 - \mu\epsilon 3\kappa m c_1]\sinh(mz). \tag{74}$$

E. Boundary layer solution

To find the boundary layer solution, we assume that the incident beam on the top surface is collimated and is directed perpendicular to the top surface, i.e., in term of (47c),

$$\mathfrak{B}(\mu, \lambda) = \delta(\mu - 1). \tag{75}$$

Using (65) and (75) yields boundary layer solution near the top surface

$$\Psi^0_{BL}(z, \mu, \lambda) = -\phi_0(0, \lambda)\int_0^1 H^0(0^-, \mu, \lambda; 0^+, \mu')[1 - r(\mu')]\mu' d\mu' \tag{76}$$

$$+3\epsilon\kappa\frac{d\phi_0(0, \lambda)}{dz}\int_0^1 H^0(0^-, \mu, \lambda; 0^+, \mu')[1 + r(\mu')]\mu'^2 d\mu' + H^0(0^-, \mu, \lambda; 0^+, 1).$$

Similarly, using (67) yields the boundary layer solution near the bottom surface

$$\Psi^1_{BL}(z,\mu,\lambda) = \phi_0(z_1,\lambda)\int_{-1}^{0} H^0(0^-,-\mu,\lambda;0^+,-\mu')[1-r(\mu')]\mu' d\mu' \tag{77}$$

$$-3\epsilon\kappa\frac{d\phi_0(z_1,\lambda)}{dz}\int_{-1}^{0} H^0(0^-,-\mu,\lambda;0^+,-\mu')[1+r(\mu')]\mu'^2 d\mu'.$$

The solution of the full problem is then

$$I = \Phi_{int} + \Psi^0_{BL} + \Psi^1_{BL}. \tag{78}$$

V. PHYSICAL INVESTIGATIONS

Below we perform a series of computational experiments of the LRTE and DABL. The LRTE is solved using the methods presented in Sec. IV A. The purpose of these investigations is twofold: to validate the asymptotics and garner physical insight into the salient features of the solutions. In particular, we focus on accurately quantifying the effects of reabsorption.

A. Reabsorption effects

To recap, when light is absorbed and reemitted, it can be reabsorbed. The probability of reemission is called the photoluminescence quantum yield and is denoted by QY. Hence, qualitatively, the loss of light flux (or photons) after n reabsorption events increases exponentially as QY^n. The asymptotic assumption leading to the diffusion approximation is that this probability is close to unity (11). However, even when the quantum yield is quite large, say, 95%, if there is a significant overlap between the absorption and reemission spectra, the reabsorption effects can be significant.

A common way to characterize this overlap is the **Stokes shift**, $\Delta\lambda_S$, which is characteristic wavelength separation between the absorption and reemission peaks. This is illustrated in Fig. 3 for the "synthetic" Gaussian spectra

$$f_r(\lambda) = \frac{e^{-\frac{(\lambda-\lambda_r)^2}{2\sigma^2}}}{\sigma\sqrt{2\pi}}, \quad f_a(\lambda) = \frac{e^{-\frac{(\lambda-\lambda_a)^2}{2\sigma^2}}}{\sigma\sqrt{2\pi}}, \tag{79}$$

where λ_a and λ_r are the central absorption and reemission wavelengths, respectively, and σ is the characteristic width of these spectra. The Stokes shift can then be defined as

$$\Delta\lambda_S = \lambda_r - \lambda_a. \tag{80}$$

Below we study the reabsorption in the LRTE and DABL for varying values of Stokes shift. We show that DABL is accurate when the Stokes shift is small. When the Stokes shift is large, DABL is, in general, not asymptotically valid. However, its results are still qualitatively accurate for wavelengths in the reemission range.

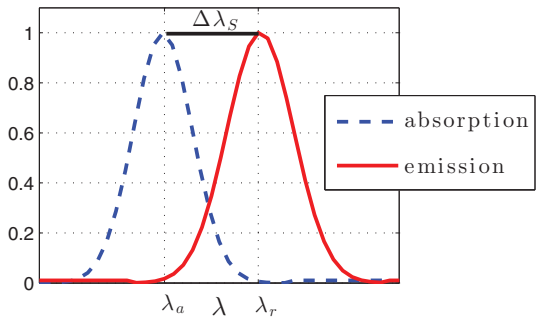

FIG. 3. Schematic absorption (dashes) and reemission (solid) spectra. $\Delta\lambda = \lambda_r - \lambda_a$ denotes the Stokes shift.

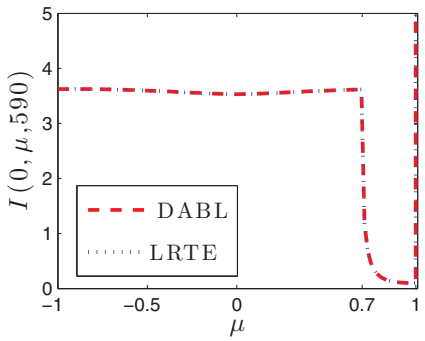

FIG. 4. Radiance on the top surface a function of the cosine angle computed directly using the LRTE (dots) and DABL (dashes). Here, $\epsilon = 0.01$, $g = 0.8$, $\lambda_a = 545$, $\lambda_r = 590$, and $\Delta\lambda_S \approx \frac{\sigma}{3}$.

In our computations, we consider a slab with $z = 0$ and $z_1 = 1$ and the relative refractive index as $n_{rel} = 1.4$. We use the Fresnel reflection coefficient for unpolarized light, given by

$$r(\mu) = \begin{cases} \frac{1}{2} \mid \frac{(n_{rel}\mu_t - \mu)}{(n_{rel}\mu_t + \mu)} \mid^2 + \frac{1}{2} \mid \frac{(n_{rel}\mu - \mu_t)}{(n_{rel}\mu + \mu_t)} \mid^2, & \mu > \mu_c \\ 1, & \mu \le \mu_c \end{cases}, \tag{81}$$

where the cosine angle of the transmitted radiation is

$$\mu_t = \sqrt{1 - n_{rel}^2(1 - \mu^2)}$$

and the cosine of the critical angle is $\mu_c = \sqrt{1 - \frac{1}{n_{rel}^2}}$.

1. Small Stokes shift

When the Stokes shift is small, i.e., in terms of (79), $\Delta\lambda_S \ll \sigma$, there is a large overlap between f_a and f_r. Therefore, the probability for reabsorption is high. This is typical for organic fluorescent particles, such as Rhodamine B (cf. Ref. 14). Specifically, in the computations below, we use (79) with $\lambda_a = 545$, $\lambda_r = 590$, and $\sigma = 150$. This corresponds to $\Delta\lambda_S \approx \frac{\sigma}{3}$.

First, we choose $\epsilon = 0.01$ and consider a forward peaked scattering phase function (50) with an anisotropy parameter $g = 0.8$. Figure 4 shows that radiances on the top surface, computed using the LRTE and DABL, as functions of the direction cosine, μ. This computation shows that DABL is very accurate. To understand this behavior of the radiance, we recall that the source is a collimated beam on the top surface pointing downwards, i.e., along the $\mu = 1$ direction. Since the medium is highly diffusive, the radiation in the directions that are close to the tangent of the boundary is largely backscattered from the medium to the top surface. This is consistent with the roughly constant radiance in the range $-1 \le \mu < 0.7$. However, much of the forward peaked radiation is transmitted outside of the medium, which is consistent with the dip of the radiance at the top surface in the range $0.7 < \mu \le 1$.

To quantify the accuracy of DABL, we use the reflectance outside of the top surface and the transmittance outside of the bottom surface, defined, respectively, as

$$\mathbf{R} = -\int_{-1}^{0} [1 - r(\mu)] I(0, \mu, \lambda) \mu d\mu, \tag{82}$$

$$\mathbf{T} = \int_{0}^{1} [1 - r(\mu)] I(z_1, \mu, \lambda) \mu d\mu. \tag{83}$$

The respective relative errors of DABL are defined as

$$\|E_{\mathbf{R}}\|_\infty = \frac{\|\mathbf{R}_{LRTE} - \mathbf{R}_{DABL}\|_\infty}{\|\mathbf{R}_{LRTE}\|_\infty}, \quad \|E_{\mathbf{T}}\|_\infty = \frac{\|\mathbf{T}_{LRTE} - \mathbf{T}_{DABL}\|_\infty}{\|\mathbf{T}_{LRTE}\|_\infty}, \tag{84}$$

where $\|\cdot\|_\infty$ is the L^∞ norm.

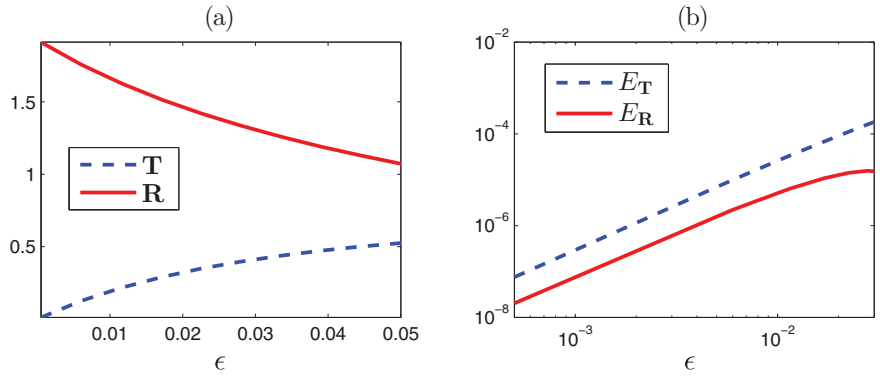

FIG. 5. (a) Reflectance [Eq. (82), solid] and transmittance [Eq. (83), dashes] evaluated at $\lambda = 590$ as functions of ϵ. All other parameters are the same as in Fig. 4. (b) Loglog plot of the relative errors [Eq. (84)].

It is interesting to study the behavior of the solutions and errors as ϵ varies. Figure 5(a) shows that, ϵ increases, the reflectance decreases while the transmittance increases. To understand this, we recall that as ϵ increases, the fluorescence (reemission) becomes larger [see Eq. (12)]. Since, in addition, the fluorescence is highly forward peaked ($g = 0.8$), as ϵ increases it is expected that the transmittance will increase and the reflectance will decrease.

Figure 5(b) shows the error of DABL *vs.* the LRTE as functions of ϵ. This result shows that the error of DABL scales as ϵ^2. Hence, this result shows that the accuracy of DABL is consistent with the asymptotic theory.

We also study the effect of anisotropy of the reemission phase function (6). To do so, we vary the anisotropy parameter from $g = 0$ (isotropic) to $g = 1$ (forward peaked reemission). Figure 6(a) shows that the reflectance decreases and transmittance increases as the reemission becomes more forward peaked. Figure 6(b) shows the associated errors of reflectance and transmittance as a function of anisotropy parameter. Both errors are found to be in the order of ϵ^2.

2. Large Stokes shift

It is also interesting to study the case of large Stokes shifts. In this case, the reabsorption cross-section is small and, therefore, the probability of reabsorption is small. This is the case for certain fluorescent semiconductor particles (cf. Ref. 15).

To study this case, we use (79) with $\lambda_a = 540$, $\lambda_r = 690$, $\sigma = 150$. This corresponds to a Stokes shift (80) $\Delta\lambda_S = \sigma$, i.e., almost no overlap between f_a and f_r. In this case, it is meaningful to define the (possibly overlapping) absorption and reemission wavelength intervals, Λ_a and Λ_r, respectively.

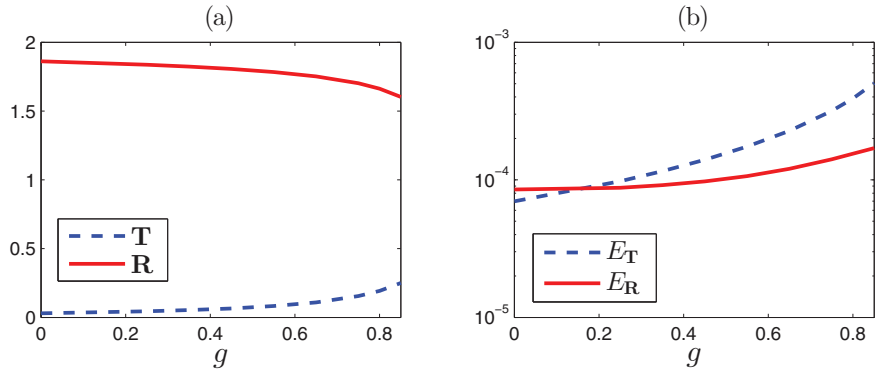

FIG. 6. (a) Reflectance (solid) and transmittance (dashes) as functions of anisotropy parameter g. All other parameters are the same as in Fig. 4. (b) Semilogy plot of the relative errors.

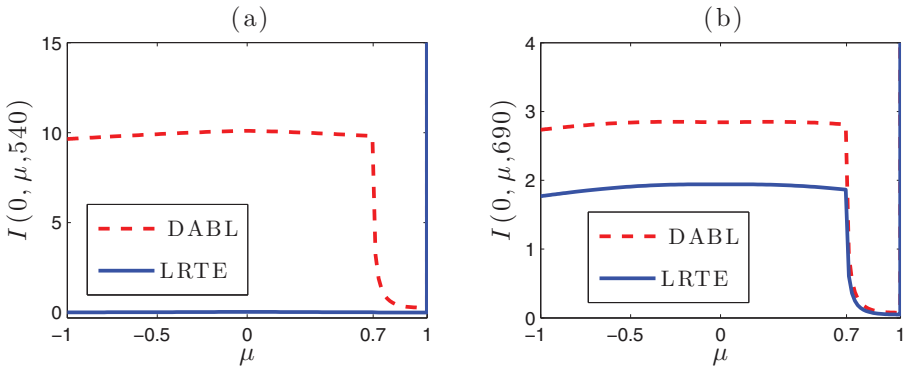

FIG. 7. The radiance on the top surface as a function of direction evaluated at (a) $\lambda = 540$ and (b) $\lambda = 690$, and computed using the LRTE (solid) and DABL (dashes). The parameters are $\epsilon = 0.01$, $g = 0.8$ and the Stokes shift is $\Delta\lambda_S = \sigma = 150$.

Figure 7 shows that DABL is generally inaccurate in this case. In particular, Fig. 7(a) shows that at $\lambda = 540$, i.e., in the absorption range, DABL is inaccurate for all μ. On the other hand, Fig. 7(b) shows that at $\lambda = 690$, i.e., the reemission range, DABL is accurate for $0.7 < \mu \leq 1$. To understand this, we note that assumption (1) do not hold in general. In particular, since $f_a(\lambda)$ decays to zero outside some subinterval of wavelengths, $\Lambda \backslash \Lambda_a$. Therefore, $f_r/f_a = o(\epsilon^{-1})$ and [from (10)] that $\mathcal{L} = \mathbb{I} + o(\epsilon^{-1})$ in $\Lambda \backslash \Lambda_a$, which invalidates the asymptotic scaling of (12). This explains the failure of the diffusion approximation in the large Stokes shift regime.

Furthermore, in the limiting case of a very large Stokes shift, i.e., when the overlap between the absorption and reemission intervals is negligible, the LRTE (1) can be broken up into a system of two coupled RTEs for the absorption and reemission as

$$\Omega \cdot \nabla I + \mu_a f_a(\lambda) I = 0, \quad \lambda \in \Lambda_a, \tag{85a}$$

$$\Omega \cdot \nabla I = \mu_a Q Y f_r(\lambda) \int_{\Lambda_a} \int_{S^2} f_a(\lambda') P_r(\Omega \cdot \Omega') I(\mathbf{x}, \Omega', \lambda')\, d\Omega' d\lambda', \quad \lambda \in \Lambda_r. \tag{85b}$$

We remark that similar systems, and associated systems of two coupled diffusion approximations, have been studied (cf. Refs. 19, 21–25). However, System (85) is physically accurate only when the reabsorption is negligible. Moreover, as mentioned above, **the diffusion approximation is not asymptotically valid in this case**. This can also be demonstrated in detail as follows. The solution of (85a) in a parallel slab with the same boundary conditions as in Sec. IV is

$$I(z,\mu,\lambda) = \begin{cases} \delta(\mu-1)\left[1 + r^2(\mu) e^{-\frac{2\mu_a f_a(\lambda)}{\mu}}\right]^{-1} e^{-\frac{\mu_a f_a(\lambda) z}{\mu}}, & 0 < \mu \leq 1, \\ \delta(\mu-1) r(\mu)\left[1 + r^2(\mu) e^{-\frac{2\mu_a f_a(\lambda)}{\mu}}\right]^{-1} e^{-\frac{\mu_a f_a(\lambda)(z+2)}{\mu}}, & -1 \leq \mu < 0, \end{cases} \tag{86}$$

where $\lambda \in \Lambda_a$ and $z \in [0, 1]$. Using the scaling (1), it follows directly from (85a), as well as from (86), that, apart from the forward peaked direction ($\mu = 1$), for $\lambda \in \Lambda_a$ the radiance scales as $\mathcal{O}(e^{-1/\epsilon})$. This is consistent with the very small LRTE solution as shown in Fig. 7(a). A similar analysis shows that the diffusion approximation is also inaccurate for $\lambda \in \Lambda_r$, apart from the forward peaked direction; and this too is shown in Fig. 7(b).

3. Varying the Stokes shift

Since DABL is, in general, only accurate for small Stokes shifts, it is interesting to study its accuracy as the Stokes shift varies. To do this, we fix $\epsilon = 0.01$, $g = 0.8$, $\lambda_r = 690$, and $\sigma = 150$, while allowing λ_a – and hence $\Delta\lambda_S$ – to vary (i.e., $\lambda_a \in [540, 690]$) .

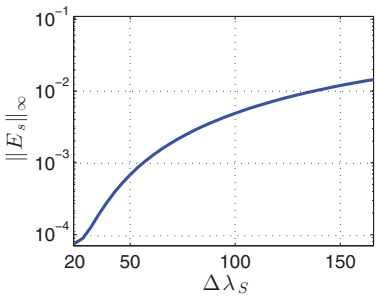

FIG. 8. Semilogy plot for the relative error in L^∞-norm as a function of Stokes shift. The parameters are $\epsilon = 0.01$, $g = 0.8$, and $\Delta\lambda_S \in [0, \sigma]$, where $\sigma = 150$.

Figure 8 shows the error of DABL for variable Stokes shifts computed for the averaged radiance on the top surface at the center of the reemission spectrum, i.e.,

$$\|E_S(\lambda_r)\|_\infty = \frac{\|\mathcal{U}_{LRTE} - \mathcal{U}_{DABL}\|_\infty}{\|\mathcal{U}_{LRTE}\|_\infty},$$

where, for either the LRTE or DABL,

$$\mathcal{U}(\lambda_r) = -\int_{-1}^{0} I(0, \mu', \lambda_r)\mu' d\mu'. \tag{87}$$

This figure shows that for $\Delta\lambda_S < \frac{\sigma}{3}$ the error of DABL is on the order of $\mathcal{O}(\epsilon^2)$, whereas, for $\Delta\lambda_S \geq \sigma$, the error beyond this scaling. This is further indication that the diffusion approximation can become inaccurate whenever the reabsorption is weak, i.e., when the overlap between f_a and f_r is small.

B. Using measured luminescence data

To further test the accuracy of DABL, we compute the solutions using measured luminescence data for semiconductor CdSe/CdTe nanoparticles [see Fig. 9(a)]. Unlike the previously used synthetic spectral data (79), here it is less clear how to define the Stokes shift. Nonetheless, over the entire range of wavelengths, the reabsorption cross-section is relatively small due to the large absorptivity at shorter wavelengths. In addition, the source function on the top surface is taken as

$$\mathfrak{B}(\mu, \lambda) = f_{sol}(\lambda)\delta(\mu - 1), \tag{88}$$

where $f_{sol}(\lambda)$ is the normalized typical average irradiance spectrum at sea level,[50] as shown in Fig. 9(a). Using the parameters $\epsilon = 0.01$, $g = 0.8$ we compute the solution of the LRTE, DABL,

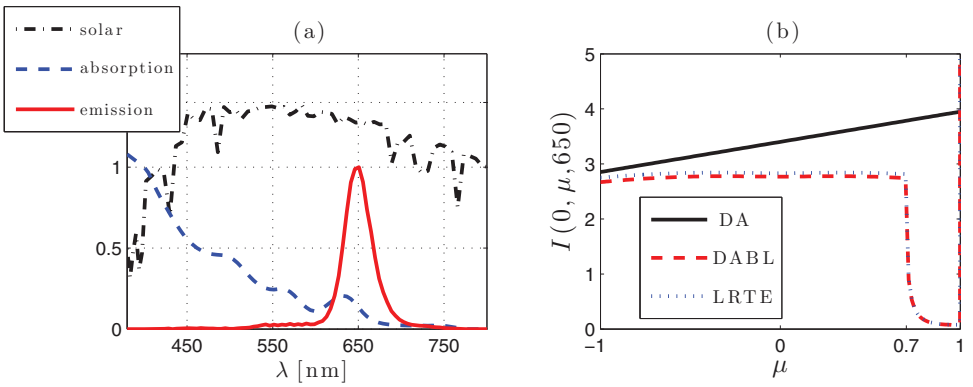

FIG. 9. (a) Solar irradiance at sea level (dot-dashes), measured absorption (dashes), and measured reemission (solid) spectra of CdSe / CdTe semiconductor nanoparticles.[15] (b) Radiance on the top surface at $\lambda = 650$ nm, computed using the diffusion approximation [see (34)], DABL (dashes), and the LRTE (dots). The parameters are $\epsilon = 0.01$, $g = 0.8$.

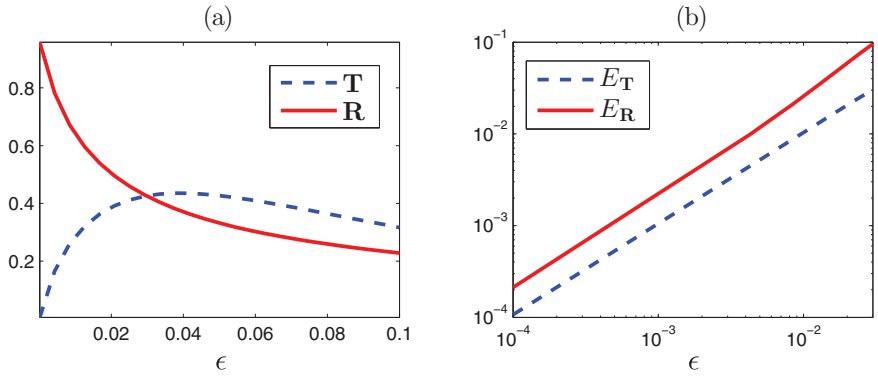

FIG. 10. (a) and (b) Same as Fig. 5 using the measured data in Fig. 9 and computed at $\lambda = 650\,\text{nm}$.

and also the (interior) diffusion approximation without the boundary layer solution but using the asymptotically accurate boundary conditions [see (34)].

Figure 9(b) shows the radiance on the top surface at $\lambda = 650\,\text{nm}$, i.e., at the center of the reemission spectrum. This plot shows that DABL is accurate compared with the LRTE. However, the diffusion approximation is inaccurate. Hence, **this result further indicates the importance of including the asymptotic boundary layer solution near the top surface.** Similar to Fig. 4, since the medium is highly diffusive, much of the radiance is backscattered from the medium to the top surface, which is consistent with the roughly constant radiance in the range $-1 \leq \mu < 0.7$. However, much of the forward peaked radiation gets transmitted outside of the medium, which explains the low radiance at the top surface in the range $0.7 < \mu \leq 1$.

Similar to Fig. 5(a), Fig. 10(a) shows that the reflectance decreases and the transmittance increases as ϵ increases. However, unlike Fig. 5(b), Fig. 10(b) shows that the errors in the reflectance do not scale as $\mathcal{O}(\epsilon^2)$. In fact, the errors appear to scale as $\mathcal{O}(\epsilon)$, though this is not guaranteed by the asymptotic theory. This reduced accuracy due to the small reabsorption, as discussed in Secs. V A 2 and V A 3. Notwithstanding this limitation, these results indicate that DABL can be qualitatively "in the ballpark" even beyond its formal regime of validity, which could be useful for inverse problems arising in fluorescence imaging and other applications.

VI. SUMMARY AND CONCLUSIONS

In this study, light transport in a luminescent medium is studied in the highly scattering (optically thick) regime. Using asymptotic matched expansion techniques, the LRTE (1) is reduced to the diffusion approximation with associated boundary conditions for the interior of the medium, and the boundary layer solution. This entire solution, called DABL, is shown to be accurate to $\mathcal{O}(\epsilon)$ globally, where ϵ is the small parameter in the problem. Using accurate numerical computations of the LRTE and DABL, we show that DABL is accurate when the Stokes shift is small. When the Stokes shift is large, DABL is, in general, not asymptotically valid. However, our computations show that, even for a large Stokes shift, DABL can be qualitatively reliable for wavelengths in the reemission range. This is the first detailed study of the reabsorption effects in optically thick media and the accuracy of the diffusion approximation in capturing these effects. The results of this study are encouraging for using DABL to solve these problems. This approach may be beneficial for solving realistic problems that arise in applications, such as modeling luminescent solar concentrators and fluorescence optical tomography.

ACKNOWLEDGMENTS

This research is supported by the National Science Foundation (NSF) under Grant No. CHE-0934615. The authors would like to thank Arnold D. Kim for many helpful discussions on the asymptotic theory and computational techniques.

[1] S. Chandrasekhar, *Radiative Transfer* (Dover Publications, Inc., 1960).
[2] K. M. Case and P. F. Zweifel, *Linear Transport Theory* (Addison-Wesley, 1967).
[3] A. Ishimaru, *Wave Propagation and Scattering in Random Media* (Wiley-IEEE-Press, 1999).
[4] G. Pomraning, *The Equations of Radiation Hydrodynamics*, International Series of Monographs in Natural Philosophy Vol. 54 (Pergamon Press, 1973).
[5] E. E. Lewis and W. F. J. Miller, *Computational Methods of Neutron Transport* (Wiley, 1984).
[6] T. Jevremovic, *Nuclear Principles in Engineering* (Springer, 2009).
[7] A. K. Prinja and E. W. Larsen, "General principles of neutron transport," in *Handbook of Nuclear Engineering*, edited by D. Cacuci (Springer, USA, 2010), pp. 427–542.
[8] S. Dhami *et al.*, Photochem. Photobiol. **61**, 341 (1995).
[9] R. Philip, A. Penzkofer, W. Bumler, R. Szeimies, and C. Abels, J. Photochem. Photobiol. A **96**, 137 (1996).
[10] J.-M. I. Maarek, D. P. Holschneider, and J. Harimoto, J. Photochem. Photobiol. B **65**, 157 (2001).
[11] Y.-C. Chen, Z. Wang, M. Yan, and S. A. Prahl, Luminescence **21**, 7 (2006).
[12] B. Heeg, P. A. DeBarber, and G. Rumbles, Appl. Opt. **44**, 3117 (2005).
[13] X. Wang *et al.*, Appl. Opt. **46**, 8446 (2007).
[14] V. Sholin, J. D. Olson, and S. A. Carter, J. Appl. Phys. **101**, 123114 (2007).
[15] D. Şahin, B. Ilan, and D. Kelley, J. Appl. Phys. **110**, 033108 (2011).
[16] J. Swartling, A. Pifferi, A. M. K. Enejder, and S. Andersson-Engels, J. Opt. Soc. Am. A **20**, 714 (2003).
[17] Y.-C. Chen, J. J. Brazier, M. Yan, P. R. Bargo, and S. A. Prahl, Sens. Actuators B **102**, 107 (2004), Selected papers from Transducers 03.
[18] M. S. Patterson and B. W. Pogue, Appl. Opt. **33**, 1963 (1994).
[19] C. Hutchinson, J. Lakowicz, and E. Sevick-Muraca, Biophys. J. **68**, 1574 (1995).
[20] D. Y. Paithankar, A. U. Chen, B. W. Pogue, M. S. Patterson, and E. M. Sevick-Muraca, Appl. Opt. **36**, 2260 (1997).
[21] G. Y. Panasyuk, Z.-M. Wang, J. C. Schotland, and V. A. Markel, Opt. Lett. **33**, 1744 (2008).
[22] A. D. Zacharopoulos, P. Svenmarker, J. Axelsson, M. Schweiger, S. R. Arridge, and S. Andersson-Engels, Opt. Express **17**, 3042 (2009).
[23] C. T. Xu, J. Axelsson, and S. Andersson-Engels, Appl. Phys. Lett. **94**, 251107 (2009).
[24] A. Joshi, J. C. Rasmussen, E. M. Sevick-Muraca, T. A. Wareing, and J. McGhee, Phys. Med. Biol. **53**, 2069 (2008).
[25] D. Yudovsky and L. Pilon, Appl. Opt. **49**, 6072 (2010).
[26] K. Liu, Y. Lu, J. Tian, C. Qin, X. Yang, S. Zhu, X. Yang, Q. Gao, and D. Han, Opt. Express **18**, 20988 (2010).
[27] A. D. Klose and T. Pöschinger, Phys. Med. Biol. **56**, 1443 (2011).
[28] D. Şahin and B. Ilan, J. Opt. Soc. Am. A **30**, 813 (2013).
[29] S. Leyre *et al.*, Opt. Express **20**, 17856 (2012).
[30] L. G. Henyey and J. L. Greenstein, J. Astrophys. **93**, 70 (1941).
[31] J. Duderstadt and L. Hamilton, *Nuclear Reactor Analysis* (Wiley, 1976).
[32] V. A. Markel and J. C. Schotland, J. Opt. Soc. Am. A **19**, 558 (2002).
[33] J. Heino, S. Arridge, J. Sikora, and E. Somersalo, Phys. Rev. E **68**, 031908 (2003).
[34] L. Wang and H. Wu, *Biomedical Optics: Principles and Imaging* (Wiley, 2007).
[35] H. Ammari, E. Bossy, J. Garnier, W. Jing, and L. Seppecher, J. Math. Phys. **54**, 021501 (2013).
[36] W. E. Meador and W. R. Weaver, Appl. Opt. **18**, 1204 (1979).
[37] K. M. Yoo, F. Liu, and R. R. Alfano, Phys. Rev. Lett. **64**, 2647 (1990).
[38] G. Bal and L. Ryzhik, SIAM J. Appl. Math. **60**, 1887 (2000).
[39] G. Y. Panasyuk, V. A. Markel, and J. C. Schotland, Appl. Phys. Lett. **87**, 101111 (2005).
[40] R. Sanchez, J. Ragusa, and E. Masiello, J. Math. Phys. **49**, 083504 (2008).
[41] E. W. Larsen and J. B. Keller, J. Math. Phys. **15**, 75 (1974).
[42] G. J. Habetler and B. J. Matkowsky, J. Math. Phys. **16**, 846 (1975).
[43] E. W. Larsen, J. E. Morel, and W. F. Miller, Jr., J. Comput. Phys. **69**, 283 (1987).
[44] A. D. Kim, J. Opt. Soc. Am. A **28**, 1007 (2011).
[45] A. D. Kim and M. Moscoso, Multiscale Model. Simul. **9**, 1624 (2011).
[46] J. Mika, J. Quant. Spectrosc. Radiat. Transfer **11**, 879 (1971).
[47] F. Malvagi and G. C. Pomraning, J. Math. Phys. **32**, 805 (1991).
[48] R. C. Haskell *et al.*, J. Opt. Soc. Am. A **11**, 2727 (1994).
[49] R. Aronson, J. Opt. Soc. Am. A **12**, 2532 (1995).
[50] K. Emery, *Terrestrial Reference Spectra for Photovoltaic Performance Evaluation*, 2000, see http://rredc.nrel.gov/solar/spectra/am1.5.